JOURNAL OF GEOPHYSICAL RESEARCH, VOL. 108, NO. C8, 3252, doi:10.1029/2002JC001515, 2003

Long waves induced by short-wave groups over a sloping bottom

T. T. Janssen and J. A. Battjes

Section of Environmental Fluid Mechanics, Faculty of Civil Engineering and Geosciences, Delft University of Technology, Delft, Netherlands

A. R. van Dongeren

WL/Delft Hydraulics, Delft, Netherlands

Received 20 June 2002; revised 14 February 2003; accepted 17 March 2003; published 7 August 2003.

[1] The cross-shore propagation of group-bound long waves is investigated. A detailed laboratory data set from *Boers* [1996] is analyzed using primarily the cross-correlation function for a sequence of closely spaced cross-shore locations, thus visualizing the propagation of the short-wave envelope and attendant low-frequency motion in detail. The results confirm the previously observed lag of the forced subharmonics behind the short-wave envelope that increases with decreasing water depth. The forced subharmonics are found to be released and reflected at the shoreline and to propagate in offshore direction as free waves. A theoretical, linear model for the forced wave evolution accurate to first order in the relative bottom slope is presented; it predicts a bottom-slope induced, spatially varying phase shift between the short-wave envelope and forced waves which is in good agreement with the observations. The phase shift has dynamical consequences since it allows energy transfer between the short-wave groups and the forced low-frequency response. *INDEX TERMS:* 4560 Oceanography: Physical: Surface waves and tides (1255); 4203 Oceanography: General: Analytical modeling; 4546 Oceanography: Physical: Nearshore processes; 4599 Oceanography: Physical: General or miscellaneous; *KEYWORDS:* forced wave motion, wave-group forced waves, bottom-induced phase shift, observations of forced waves over variable depth

Citation: Janssen, T. T., J. A. Battjes, and A. R. van Dongeren, Long waves induced by short-wave groups over a sloping bottom, *J. Geophys. Res.*, *108*(C8), 3252, doi:10.1029/2002JC001515, 2003.

1. Introduction

[2] In coastal areas, the presence of wave motion in the infragravity band (typically, 0.004–0.04 Hz) is an important factor in the design of coastal structures and the evolution of coastal morphology. The slow modulation of the water depth may significantly affect the design wave height for structural design and represent an important factor in bar formation. Harbors and large-vessel mooring systems may experience resonance in the infragravity band; consideration of infragravity forcing may be normative to their design.

[3] *Munk* [1949] was the first to report low-frequency motion observed well outside the surf zone. He suggested it was caused by the variability of mass transport by the incident waves into the surf zone, and named it "surf beat." *Tucker* [1950] cross-correlated the short-wave envelope with the local low-frequency motion, one thousand yards offshore. The most outstanding feature in this correlation function was a negative peak at a lag approximately equal to the sum of the travel times of a wave group traveling to the shoreline and of a free wave, reflected from the shoreline, returning to the position of observation. Tucker confirmed the linear relation between swell amplitude and low-frequency amplitude reported by Munk.

[4] Although *Tucker* [1950] argued that the varying mass transport with groups of high and low waves might cause the generation of low-frequency motion, he was unable to relate this to the observed correlation. Groups of higher waves were expected to induce an enhanced shore-directed mass transport, which is incompatible with the observed negative correlation. Also, the quadratic dependence of mass transport on wave height seemed inconsistent with the observed linear relation.

[5] By solving the field equations and boundary conditions of the water wave problem accurate up to second order, *Biésel* [1952] and later *Longuet-Higgins and Stewart* [1962] showed that modulation of the wave height at the timescale of the wave groups causes a variation in the water level, usually referred to as "bound" or "forced" long waves, such that the water level is depressed under groups of high waves, the mass transport being negative there. Longuet-Higgins and Stewart explain the generation of these bound waves in terms of the variation of the radiation stresses on the time and length scales of the short-wave groups. The model derived by Longuet-Higgins and Stewart provides a mechanism consistent with the observed negative correlation. It predicts a quadratic proportionality between the amplitude of the incident primary waves and subhar-

0148-0227/03/2002JC001515$09.00

monic response with increasing response amplitude for decreasing water depth. Longuet-Higgins and Stewart argued (similar to an argument used by *Tucker* [1950]) that, since waves of smaller amplitude are allowed to propagate into shallower water, and thus are amplified more strongly, we might expect the relation between swell and low frequency to be at least weaker than quadratic (and thus closer to the observed linear one).

[6] The expression for the equilibrium bound wave amplitude in shallow water derived by *Longuet-Higgins and Stewart* [1962] can be expanded in a Taylor series for $k^{(1)}h$ ($k^{(1)}$ representing a characteristic wavenumber of the primary waves). To a first-order approximation, assuming conservative shoaling for the primary waves, this yields a forced wave amplitude variation proportional to $h^{-5/2}$. The latter limit is often interpreted as a shoaling law for forced waves over a sloping bottom, although it is based on the equilibrium response in constant depth. Note that Longuet-Higgins and Stewart do have reservations concerning the limited validity of this equilibrium solution over sloping bottoms.

[7] Assuming the surf zone wave height to be a function of local depth alone, a modulated incident wave train gives rise to excursions of the initial point of wave breaking at the time and length scale of the wave modulation. *Symonds et al.* [1982] show for a weakly modulated incident wave train that this results in radiation of free waves away from the region of initial breaking. *Symonds and Bowen* [1984] extend this model to include a barred depth profile shoreward of the breaking region, allowing a half-wave resonance in that region; in particular they investigate the coincidence of this resonance condition with that of the quarter-wave resonance of the moving breakpoint mechanism. Both models neglect incident forced low-frequency wave motion, but they are linear in the description of the low-frequency motion, which allows superposition of solutions.

[8] *Schäffer* [1993] presents a semi-analytical model that combines long-wave generation due to variations in the initial breakpoint position with local forcing due to modulations of the primary waves both inshore (partial transmission of modulation) and offshore of the breakpoint for a plane sloping beach. Several numerical models, capable of modeling the forcing of subharmonic wave motion by considering spatial gradients in the radiation stress function, were developed and reported [e.g., *Van Leeuwen and Battjes*, 1990; *Van Leeuwen*, 1992; *List*, 1992; *Roelvink*, 1993; *Van Dongeren and Svendsen*, 2000; *Reniers et al.*, 2002].

[9] Laboratory experiments performed by *Kostense* [1984] on a relatively steep beach (1:20) showed some qualitative but poor quantitative agreement with predictions of the *Symonds et al.* [1982] model. *Mansard and Barthel* [1984] report observations that suggest a domination of locally forced waves accompanying (but lagging) the short-wave groups while propagating over a sloping bathymetry. *Baldock et al.* [2000] performed laboratory experiments on a steep beach (1:10), and their observations of low-frequency motion were mainly attributed to the time variation of the initial breakpoint [see also *Baldock and Huntley*, 2002].

[10] In the field, the generation and propagation of low-frequency motion in the nearshore region is complicated due to the two-dimensional nature of the wave field and bed topography. Refractive trapping of long waves may occur, resulting in edge waves [e.g., *Gallagher*, 1971; *Bowen and Guza*, 1978]. Field observations [e.g., *Elgar et al.*, 1992; *Okihiro et al.*, 1992; *Herbers et al.*, 1994; *Ruessink*, 1998] suggest that low-frequency motion, as present in the observations, is usually a combination of locally generated free and forced components. Also, these observations support an increasing dominance of forced waves (relative to the total infragravity wave field) with more energetic seas and swell.

[11] The effects of a varying bathymetry on the subharmonic response, in particular the radiation of free waves away from a local region of varying depth, is studied by *Molin* [1982] for normal wave incidence and deep water conditions for the primary (forcing) waves. This is extended by *Mei and Benmoussa* [1984] for obliquely incident waves and intermediate water depth for the forcing waves ($k^{(1)}h = O(1)$), based on a WKB expansion described by *Chu and Mei* [1970]. Part of this is re-examined by *Liu* [1989].

[12] *Bowers* [1992] and *Van Leeuwen* [1992] analytically express the effect of the depth gradient on the local, forced response as a perturbation of the flat bottom situation. The inclusion of depth variations appears to give rise to a spatially varying phase shift between the local response and the forcing short-wave groups; it provides a theoretical explanation for the changing phase relation observed in the laboratory [e.g., *Mansard and Barthel*, 1984; *Van Leeuwen*, 1992; *Janssen et al.*, 2000], in the field [e.g., *Elgar and Guza*, 1985; *List*, 1992; *Masselink*, 1995], and in numerical studies [e.g., *List*, 1992; *Herbers and Burton*, 1997].

[13] A phase shift between the primary wave envelope and forced subharmonics (away from the π radians phase difference) has important consequences for the evolution of the system of primary waves and locked subharmonics since it is a necessary condition for net energy exchanges to occur. This aspect has received little attention so far [see, e.g., *Van Dongeren*, 1997; *Van Dongeren et al.*, 2002]. The present work is aimed at improving our understanding and modeling of the relation between the short-wave envelope over a sloping bottom and the induced low-frequency motion, with emphasis on the phase lag. We will analyze a laboratory data set reported by *Boers* [1996] with an exceptionally high spatial resolution. Wave gauge data are analyzed utilizing the cross-correlation function. The high resolution of the experimental data allows a detailed visualization of the spatial evolution of this cross-correlation function, which appears to be particularly well suited for a qualitative analysis of the propagation of the short-wave envelope, the low-frequency motion, and their relation. The observed changing phase relation between the forced low-frequency motion and the short-wave envelope for a 1-D situation is explained and satisfactorily predicted on the basis of a perturbation expansion of the linearized shallow-water equations for waves over a sloping bottom.

[14] In section 2 we describe the experimental set-up used by *Boers* [1996] along with our analysis techniques. The results are presented and discussed in section 3. The mathematical model is presented in section 4 where, also, the results for the bottom slope-induced phase shift between

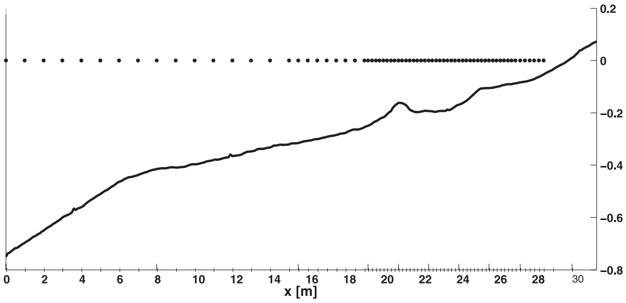

Figure 1. Beach profile, positive x direction from left to right. Dots at SWL and x axis ticks indicate wave gauge positions.

response and forcing are compared to the observations. We conclude with a discussion in section 5 and conclusions in section 6.

2. Experimental Arrangement and Method of Analysis

[15] In this section we describe the experimental arrangement used by *Boers* [1996] and our method of analysis.

2.1. Experimental Set-Up

[16] *Boers* [1996] conducted experiments in a 40-m-long, 0.8-m-wide wave flume of the Fluid Mechanics Laboratory, Department of Civil Engineering and Geosciences at Delft University of Technology. The flume was equipped with a hydraulically driven, piston-type wave generator. The bottom profile used in the experiments, molded in sand with a smooth concrete surface, is shown in Figure 1 (a model of a barred sandy beach to fit the purposes of Boers' experiments). The origin of the x axis is at the beginning of the slope, where, also, the wave gauge nearest to the wave board was positioned. The mean position of the wave generator is at $x = -4.5$ m relative to this origin. The dots at SWL and the marks along the x axis indicate the 70 wave gauge positions with corresponding x positions x_i, $i \in \{1..70\}$. As can be seen from this figure the spatial resolution is highest (0.2 m) in the nearshore region (19 m $\leq x \leq$ 28.5 m).

[17] The control signal for the wave board was a relatively short duration, irregular wave signal repeated several times. The wave signal cycle periods, together with significant wave height, H_s, and peak period, T_p, for the three experiments considered here, are shown in Table 1; it can be seen that the duration of the signal is approximately 75 times the peak period of the signal. Experiments 1A and 1B both have peak periods of approximately 2 s, while the peak period of experiment 1C is considerably higher (3.3 s). In terms of wave steepness, experiment 1B is an extreme in the set of experiments followed in decreasing order by 1A and 1C. To avoid confusion, we use the labels of the experiments as given by *Boers* [1996], but since the phenomena we want to emphasize are most eminent in experiment 1C (low wave steepness), we focus on those results and refer to 1A and 1B mainly where these show significant differences.

[18] The wave board control signal was accurate up to second order in wave steepness [*Klopman and Van Leeuwen*, 1992] to suppress generation of spurious higher and lower harmonics; active reflection compensation (ARC) was in operation to minimize re-reflections at the wave board. However, in view of restrictions imposed by the limited excursion of the wave board, the signals used in the ARC were high-pass filtered at $f_p/5$ for experiment 1B and at $f_p/10$ for experiments 1A and 1C. The deterministic wave board control signal was used for multiple repetitions of runs with identical input signals so as to cover a wide cross-shore interval with high spatial resolution (70 positions) using a limited number of wave gauges. Surface elevation records were typically 30 min long and acquired at 20 Hz.

2.2. Method of Analysis

[19] We separate recorded surface elevation signals $\eta(t)$ into low-frequency (lf) and high-frequency (hf) components, denoted by $\eta^{\mathrm{lf}}(t)$ and $\eta^{\mathrm{hf}}(t)$, respectively. The superscripts lf and hf relate to frequency ranges f_n, $n \in \{1..p/2 - 1\}$ and $n \in \{p/2..2p\}$, respectively, where p denotes the counter corresponding to the peak frequency, f_p.

[20] Since we are interested in the variation of wave amplitude on the timescale of the wave groups, we define an hf-envelope function over the observed time series $\eta^{\mathrm{hf}}(t)$ as

$$|A(t)| = \left|\eta^{\mathrm{hf}}(t) + i\Gamma\{\eta^{\mathrm{hf}}\}\right|^{\mathrm{lf}}, \tag{1}$$

where Γ {} denotes the Hilbert transform operator. This operator applies a frequency independent phase shift of $\pi/2$ to the signal it operates on [e.g., *Bendat and Piersol*, 1986; *Lancaster and Šalkauskas*, 1996]. For the case where the original signal represents a relatively narrow band process, the time series of this absolute value, $|A(t)|$, can be interpreted as the envelope of the original signal. An example of an envelope function obtained through the operation of equation (1) is shown in Figure 2.

[21] The basis of our analysis is the well-known cross-correlation function. The high spatial resolution of the experimental data allows a presentation of the sequence of correlation functions as quasi-continuous in space. In this section we introduce the different cross-correlations used in this paper and the corresponding notation. For any two real signals $V(t)$ and $Y(t)$ of a random, stationary process with zero mean, a correlation function can be defined [e.g., *Bendat and Piersol*, 1986; *Oppenheim and Schafer*, 1989] as

$$R_{VY}(\tau) = \frac{\langle V(t)Y(t+\tau)\rangle}{\sigma_V\sigma_Y}, \tag{2}$$

where $\langle .. \rangle$ denotes a time averaging operator and τ denotes a time shift. The σ_V and σ_Y are standard deviations of $V(t)$ and $Y(t)$, respectively, and $-1 \leq R_{VY} \leq 1$. We apply the cross-correlation technique to various combinations of signals and positions and use a corresponding notation to distinguish

Table 1. Experimental Program, Wave Height, and Peak Period as Observed at x = 0 m, Taken From *Boers* [1996]

Name	H_s, m	T_p, s	Cycle Period, s
1A	0.16	2.05	157.079
1B	0.21	2.03	157.079
1C	0.10	3.33	245.441

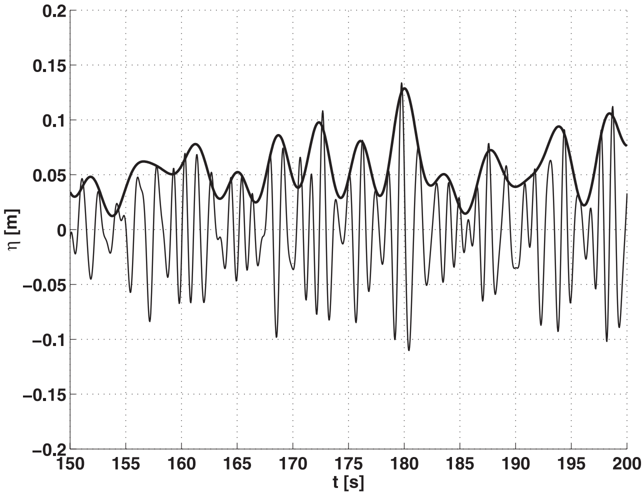

Figure 2. Example of wave envelope, $|A(t)|$, obtained through application of the Hilbert transform operator on η^{hf}. Thin line: short-wave surface elevation, η^{hf}. Thick solid line: short-wave envelope, $|A(t)|$, computed as in equation (1).

between them. The set R_{VY} (τ, x_i) denotes the collection of cross-correlation functions obtained by cross-correlating the signals $V(t)$ and $Y(t)$, which are simultaneously observed at x_i, $i \in \{1..70\}$. For example, the cross-correlation between the lf-signal, η^{lf} (t), and the squared envelope signal, $|A(t)|^2$, as observed at x_i, $i \in \{1..70\}$, is denoted by $R_{\eta A}$ (τ, x_i), in which the subscripts η and A correspond to η^{lf} (t) and $|A(t)|^2$, respectively. Alternatively, the set R_{VY} (τ, x_i; x_r) denotes the collection of cross-correlation functions obtained by cross-correlating signals $V(t)$ observed at x_i, $i \in \{1..70\}$ and $Y(t)$ as observed simultaneously at a fixed reference position x_r. Note that x_r is related to the second subscript on R.

[22] The values of each of these correlation functions have been plotted in the (x, τ)-plane at the discrete values of x and τ where they are available. The high resolution in space and time allows these function values to be presented on a quasi-continuous basis, made visible by a color scale, indicating regions of constant values of R in the (x, τ)-plane. Inspection of the "continuum" of cross-correlation values in the (x, τ)-plane allows recognition of ridges and troughs of significant positive or negative correlation. Since a consistent pattern in the (x, τ)-plane of the cross-correlation function is likely to be caused by a physical phenomenon, rather than by noise, this quasi-continuous presentation supports the identification of significant peaks and dips that may not be recognized as such when studying the individual correlation functions.

3. Results and Discussions

[23] Prior to relating the lf-waves to the squared envelope, we present the results for the cross-correlation functions for each of these signals separately, to investigate their propagation and transformation through the flume.

3.1. Short-Wave Envelope Evolution

[24] Figure 3 shows the cross-correlation between the squared envelope signal, $|A(t)|^2$, obtained from time series of experiment 1C at each individual position and as observed at Station 1 (x = 0 m), denoted as R_{AA} (τ, x_i; x_r = 0 m). In the figure the cross-lines at the vertical axis indicate wave gauge positions whereas the solid white line presents τ = 0 s.

[25] The presence of a single dominating bar of positive correlation in Figure 3 indicates that the squared envelope propagates shoreward, is destroyed in the process of breaking of the hf-waves, and is not reflected in offshore direction, which confirms the usual assumption. The dashed marker line in the figures indicates time lag values for a signal propagating at the (linear theory) group velocity, C_{gp}, corresponding to the peak frequency, f_p (steady set-up was measured and local water depth was corrected accordingly for all numerical comparisons to observed time lags). The computed lags agree very well with the observed lags of maximum correlation, thus confirming that C_{gp} is a good approximation of the actual celerity of the squared envelope, C_A.

[26] The hf-envelope propagates in onshore direction and undergoes only minor changes (dispersion effects) up to the breaker bar near x = 21 m, where the maximum value of the cross-correlation function decreases rapidly. The hf-envelope is either destroyed in the breaking process over the bar or transformed significantly. The negative correlation observed shoreward of x = 25 m in the continuation of the main correlation bar, indicates an inversion of the groupiness. The latter implies that on average the highest wave before breaking is the lowest after breaking, as inferred by *Schäffer* [1993] and in agreement with observations reported by *Veeramony and Svendsen* [1996].

[27] Figure 4 shows similar results, R_{AA}(τ, x_i; x_r = 0 m), for experiment 1B, again with the reference station at x = 0 m. This experiment is an extreme in the sets of experiments (steep waves). The higher wave steepness clearly reduces the length of the bar of high positive correlation compared to the milder case of experiment 1C. Wave breaking was observed to occur throughout the flume (M. Boers, personal communication, 2000), apparently inducing a rapid trans-

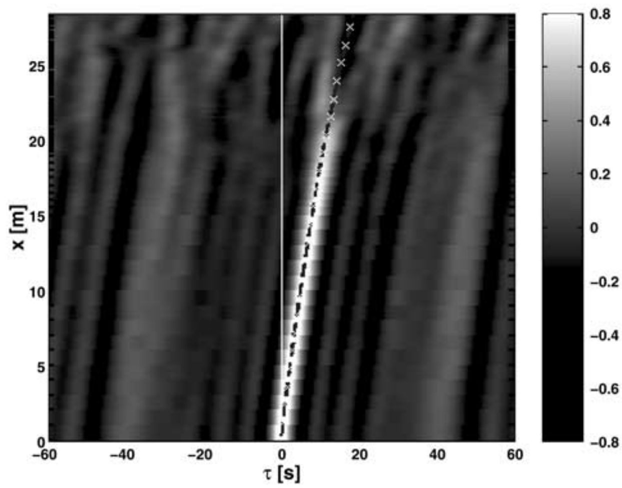

Figure 3. Cross-correlation functions of the squared short-wave envelope, R_{AA}(τ, x_i; x_r = 0 m), for experiment 1C. Dashed marker line indicates time lag values for signal propagating at group speed, C_g, corresponding to f_p.

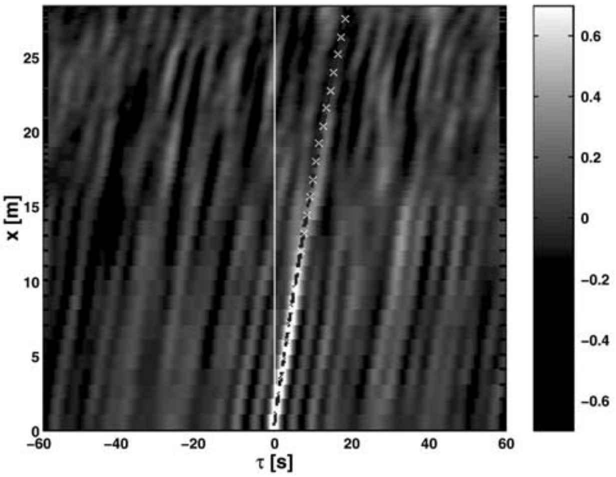

Figure 4. Cross-correlation functions of the squared short-wave envelope, $R_{AA}(\tau, x_i; x_r = 0\text{ m})$, for experiment 1B. Dashed marker line indicates time lag values for signal propagating at group speed, C_g, corresponding to f_p.

formation of the hf-envelope even prior to reaching the actual surf zone. We hypothesize that this also explains that no inversion of groupiness is observable when cross-correlating with the most offshore station.

3.2. Evolution of Low-Frequency Waves

[28] In Figures 5a and 5b the values of the cross-correlation function of the lf-surface elevation, $R_{\eta\eta}(\tau, x_i; x_r)$, for experiment 1C are shown. The reference locations are x_r = 0 m and x_r = 19.2 m for Figures 5a and 5b, respectively. In both figures a comparison is made with computed time lag values for an incident signal propagating with C_{gp}, reflected at the still-water line at x = 30 m and propagating in offshore direction at the free shallow water wave celerity ($\sqrt{gh}$). Note that the curves are not symmetric, due to the fact that the groups of primary waves propagate at C_{gp} (for f_p), which is less than the long-wave velocity, except for the limit of shallow water. Note also the mismatch between the bar of positive correlation with positive gradient ($dx/d\tau$) and the computed time lag values for the incident signal. The gradient of the bar corresponding to the observed lf-signal is slightly smaller than that corresponding to C_{gp}, indicating that, at least for some regions, the actual celerity of the lf-signal, C_{lf}, is smaller than C_{gp}. In both figures it can be seen that $\sqrt{gh}$ is a good approximation for the propagation velocity of the outgoing lf-waves.

[29] The fact that in Figures 5a and 5b the ridges of high correlation extend from x = 0 m all the way to the most shoreward station (x = 28.5 m), whereas no ridges appear to originate from $x \approx 21$ m (near the breaker bar in the bottom profile), indicates absence of significant reflection or radiation of lf-energy at the breaker bar. This signifies that the outgoing lf-motion predominantly consists of shoreline reflections of incident wave motion. Its distinctness justifies the notion of reflection at a discrete location (coinciding with the shoreline).

[30] In Figure 5a we notice two asymmetric inverted "V"-like patterns centered around τ = 0 s (notice that the reference station is at x = 0 m). Although this may seem a contradiction of causality, a closer analysis reveals otherwise. Consider a wave pulse propagating in positive x direction, partly reflected at x = 30 m, say. Figure 6a shows the (artificial) time records at x = 0 m and x = 18 m (solid and dashed lines, respectively). Figure 6b shows their cross-correlation. The strongest correlation occurs for such (positive) lag or time shift that the incident wave signals basically overlap (indicated as region 1 in Figure 6b). Likewise, a significant but weaker correlation occurs for such (negative) shift (Figure 6b, region 2) that the reflected signals at the two positions overlap. However, since the returning signal is a reflection of the incident one, these, too, are correlated for those shifts for which they overlap, giving rise to two more peaks of significant correlation (regions 3

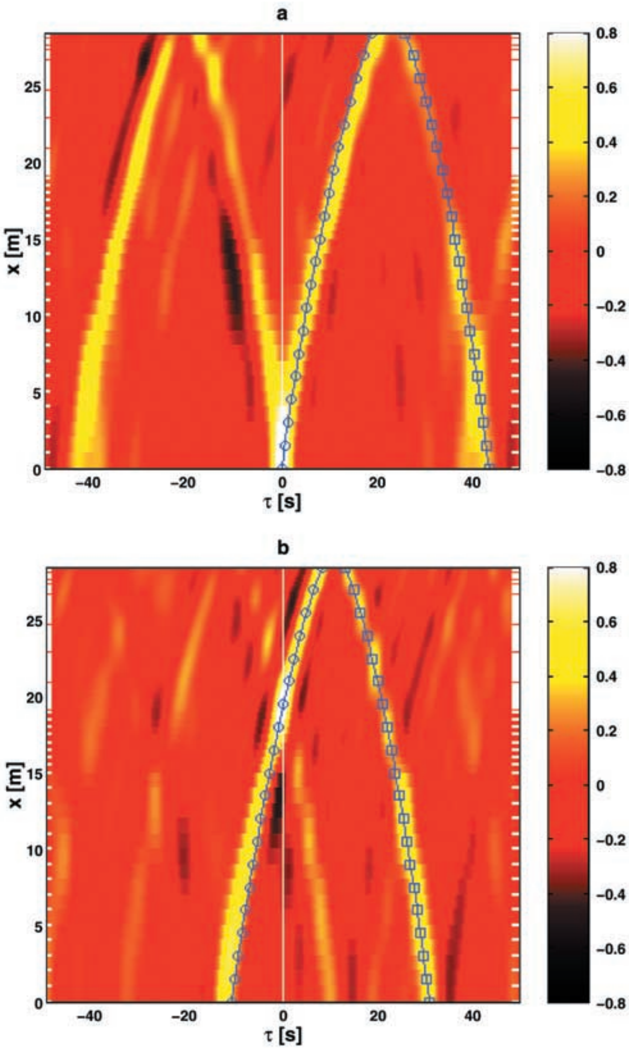

Figure 5. Correlation functions of the low-frequency motion, $R_{\eta\eta}(\tau, x_i; x_r)$, as observed in experiment 1C. Lines with circular markers indicate time lag values for signal propagating in shoreward direction at group speed, C_{gp} (for f_p). Lines with square markers indicate time lag values corresponding to signal reflected at x = 30 m propagating in offshore direction at $\sqrt{gh}$. (a) Reference position x_r = 0 m. (b) Reference position x_r = 19.2 m.

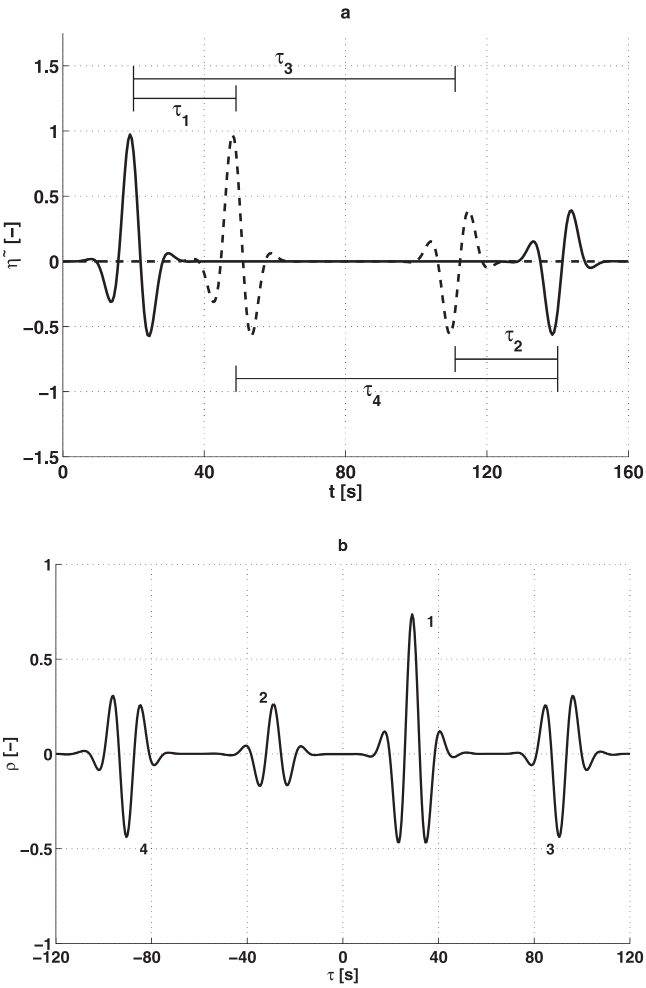

Figure 6. Numerical example to elucidate appearance of "doubled" cross-correlation peaks (and thus ridges in $x - \tau$ presentation). (a) Thick, solid line represents an incident pulse with compact support and its partial reflection at x = 30 m (the pulse at $\tau \approx 140$ s) as observed at location x = 0 m; the dashed line represents a similar observation at x = 18 m. (b) Cross-correlation function between signals is shown in top panel.

and 4). Altogether, we have four lag intervals of significant correlation, of which two coincide at zero lag (autocorrelation) if $x_i = x_r$ (= 0 m in Figure 5a), which explains the pattern seen in Figure 5a.

[31] Figure 5b shows $R_{\eta\eta}(\tau, x_i; x_r = 19.2 \text{ m})$, which is similar to Figure 5a for a reference position much closer to shore. A single asymmetric, inverted "V"-like pattern is predominant here, in contrast to Figure 5a. Around $x = x_r$ = 19.2 m the dominant pattern (around τ = 0 s) is the bar of positive correlation and positive gradient ($dx/d\tau$), which is interpreted as an indication of a dominance of incident lf-wave motion in the total lf-signal around this position. The near-vanishing of the second asymmetric, inverted "V" (relative to Figure 5a) can be deduced from foregoing explanations in conjunction with Figure 6, given the dominance of the incident lf-motion in the nearshore region.

[32] It is noticeable in Figure 5b that at positions farther offshore, the bar of positive correlation and negative gradient (the utmost right bar in Figure 5b) grows more distinct. This bar corresponds to the correlation between the incident lf-motion observed at $x = x_r$ = 19.2 m and the outgoing lf-waves observed at x_i, $i \in \{1..70\}$. The increasing dominance of this bar suggests that the relative contribution of the outgoing lf-motion to the total lf-variance increases farther offshore. This requires the incident and outgoing waves to grow/decay with different rates. We return to this below (section 6).

3.3. Relation Between Low-Frequency Motion and Envelope

[33] Here we investigate the local relation between the squared hf-envelope and the lf-motion and its spatial evolution. However, understanding of the behavior of the signals separately, as discussed above, is crucial in the interpretation of the results.

[34] Figure 7a shows the cross-correlations $R_{\eta A}(\tau, x_i)$ between the observed lf-motion and squared envelope at identical positions (no fixed reference location). A ridge of strong negative correlation can be observed from x = 0 m up to x = 25 m at near-zero time lag, which is in agreement with the theoretical prediction of a forced wave accompanying the short-wave groups. However, if we follow this ridge of negative correlation from x = 0 m towards $x \approx 22$ m, we notice that its center is shifted increasingly toward positive time lag with decreasing water depth; this indicates a lagging of the lf-motion behind the squared envelope. The latter observation is consistent with trends visible in Figures 3 and 5 and in agreement with previous field and laboratory observations [e.g., *Elgar and Guza*, 1985; *List*, 1992; *Masselink*, 1995; *Mansard and Barthel*, 1984; *Van Leeuwen*, 1992; *Janssen et al.*, 2000] where a similar evolution of the phase lag between forcing groups and lf-response was observed outside the surf zone.

[35] Moving farther toward the shoreline along τ = 0 s in Figure 7a, we note that close to shore the relation is essentially inverted compared to the offshore situation. Offshore, the lf-motion is negatively correlated with the short-wave groups at zero time lag while in the nearshore region the correlation at zero lag is dominantly positive. We mainly ascribe this to depth modulation by the lf-motion in the nearshore region; the depth-saturated short-waves are allowed to enter the shallow region on the crest of the lf-motion, thus causing a positive correlation. The relation between short-waves and lf-motion in the nearshore region may, to a lesser extent, also be affected by the inversion of groupiness in the breaking process and the slope-induced phase lag of the forced subharmonics behind the short-wave envelope already present outside the surf zone.

[36] In Figure 7a a comparison is made with computed time lag values corresponding to the summed travel times for a signal propagating from position x_i with C_{gp} in onshore direction, reflected at x = 30 m and returning to x_i with the free long-wave celerity (as *Tucker* [1950] did for a single position). Along this line (square marker line in Figure 7a), offshore from the location where $x \approx 21$ m, we observe strong negative correlation. This indicates that the lf-motion propagating in offshore direction is indeed free (corresponding time lags) and negatively correlated to the incident wave groups. This is consistent with the

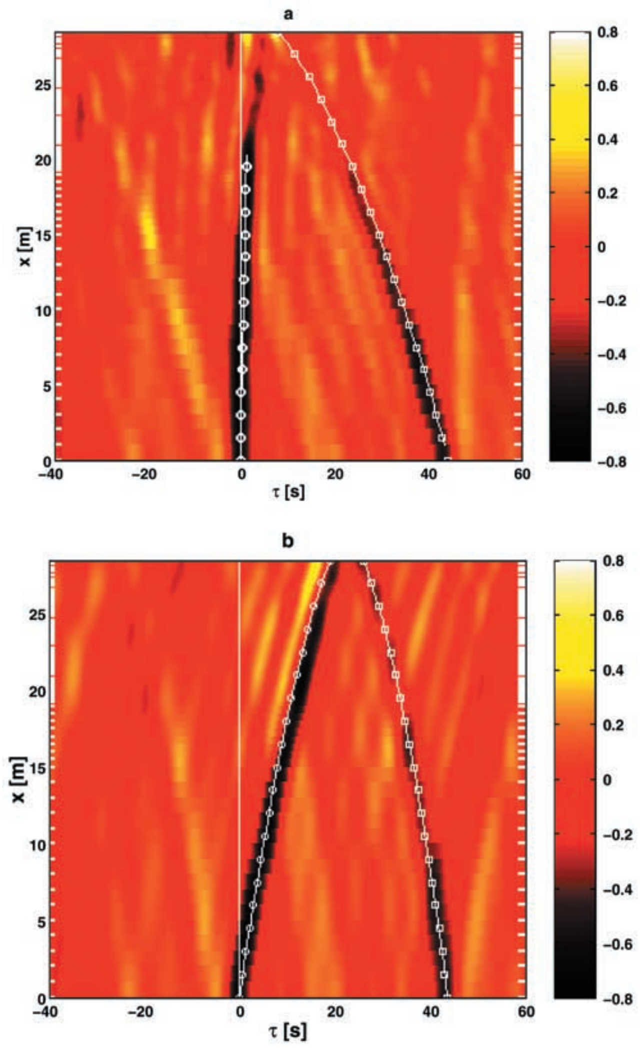

Figure 7. Cross-correlation functions between squared short-wave envelope, $|A(t)|^2$, and low-frequency motion, $\eta^{lf}(t)$, as observed in experiment 1C. (a) Signals at same position ($R_{\eta A}(\tau, x_i)$); line with circular markers indicates time lag values computed with AER model (§4); line with square markers indicates summed travel times for incident signal with celerity C_{gp} (for f_p) reflected at the shoreline (x = 30 m) and propagating seaward at celerity $\sqrt{gh}$. (b) Cross-correlation squared short-wave envelope at x = 0 m with $\eta^{lf}(t)$ at all available positions ($R_{\eta A}(\tau, x_i; x_r = 0$ m)); line with circular markers indicates time lag values for incident signal propagating at C_g (for f_p); line with square markers indicates time lag values for outgoing signal reflected at x = 30 m propagating at $\sqrt{gh}$.

release of the incident bound waves, as the short-waves are breaking, and the subsequent reflection at the shoreline. Notice that there are no indications of lf-motion being reflected or generated at the breaker bar near x = 21 m as would be predicted by the model of *Symonds et al.* [1982]. This theory predicts values of outgoing waves, induced by the breaking of weakly modulated bichromatic primary waves on a plane slope, that vary with the normalized surf zone width. Since the present analysis involves a fully modulated random wave field, we refrain from attempting to verify the applicability of this theory to our data, even in the extended version for a barred beach by *Symonds and Bowen* [1984].

[37] Inspection of the numerical values of the cross-correlation function for $x \leq 20$ m shows that the bar close to τ = 0 s (incident waves) is dominant (larger absolute values of the cross-correlation) compared to the bar corresponding to the reflected waves at all positions. However, the reflected waves become increasingly important with increasing distance offshore; in the present set-up they are almost of equal magnitude at the most offshore position of observation (x = 0 m). If this trend would extend farther offshore this could explain the observed domination of lf-waves propagating in offshore direction reported by *Tucker* [1950] without contradicting the observed incident lf-motion dominance closer to the surf zone. A similar spatial variability of the relative importance of outgoing waves is reported by *Sheremet et al.* [2002].

[38] Figure 7a may obscure the fate of the incident lf-motion in the area of significant short-wave breaking, since the breaking deforms the short-wave envelope to such extent that the lf-motion is no longer correlated to the local squared envelope. However, if the lf-motion remains relatively unperturbed, apart from being released, we may expect it to remain correlated to the squared envelope as observed offshore. In Figure 7b we show the result of cross-correlating the local lf surface elevation with the squared envelope observed at x = 0 m, $R_{\eta A}(\tau, x_i; x_r = 0$ m), for experiment 1C. We observe that in this diagram the bar of negative correlation indeed extends all the way to the most shoreward station (x = 28.5 m). This clearly indicates that the lf-waves, initially forced, persist through the zone where the short waves break, are released there, and propagate to the shoreline where they are reflected. In the surf zone, at slightly smaller lags than the bar of negative correlation, a bar of positive correlation is seen to appear. This is similar to observations reported by *List* [1992] and *Masselink* [1995]. It can be argued that this positive ridge is related to lf-motion generated in the breaking process (which is qualitatively consistent in terms of correlation and time lags). However, *List* [1992] found a similar positive peak even in the absence of breakpoint-generated waves. We hypothesize that these positive correlations are caused by the presence of free waves, positively correlated to, and preceding, the short-wave envelope, generated and radiated away while the system of primary wave groups and locally forced subharmonics propagates over an area of variable depth [e.g., *Molin*, 1982; *Mei and Benmoussa*, 1984; *Liu*, 1989; *Dingemans et al.*, 1991].

4. Mathematical Model

[39] The evolution of the cross-correlation function between the squared hf-envelope and lf-motion showed a change of phase relation between these signals while propagating over an uneven bottom well before significant wave breaking occurs. Phase shifts between forcing and response away from π, not predicted by Stokes second-order theory for a flat bottom [e.g., *Biésel*, 1952; *Longuet-Higgins and Stewart*, 1962; *Hasselmann*, 1962], were previously reported from field observations [e.g., *Elgar and Guza*, 1985; *List*, 1992; *Masselink*, 1995] and in the laboratory

[e.g., *Mansard and Barthel*, 1984; *Van Leeuwen*, 1992; *Janssen et al.*, 2000].

[40] *Bowers* [1992] and *Van Leeuwen* [1992] have shown analytically that the varying depth induces a phase shift between the primary wave envelope and low-frequency response while propagating over a varying depth. The present work is in line with *Van Leeuwen*'s [1992] approach with the exception that consistent use of multiple scales in the spatial variable leads us to include the spatial variation of the lf-amplitude, the latter being neglected by Van Leeuwen. The result is a linear evolution model for amplitude and phase of the lf-motion to first order in bottom slope.

[41] The analysis in this section is aimed at modeling the spatially varying phase shift between the short-wave envelope and incident forced subharmonics while propagating over an uneven bottom prior to breaking. The description is limited to the shoaling region of the primary waves and the accompanying incident locked harmonics; no provisions were made to include low-frequency motion induced by time variation of the initial breakpoint [*Symonds et al.*, 1982; *Symonds and Bowen*, 1984]. However, since the model is linear in the description of the low-frequency motion, solutions may be superposed.

[42] We consider a narrow-band primary wave motion expressed as a wave train modulated by a slowly varying amplitude as in

$$\eta^{(1)}(x,t) = \frac{1}{2}A(x,t)\exp[i(\psi_0(x) - \omega_0 t)] + *, \tag{3}$$

where * denotes the complex conjugate of the preceding term and the amplitude, $A(x, t)$, can be written as

$$A(x,t) = \sum_{n=L}^{U} a_n(x)\exp\cdot[i(\psi_n(x) - \psi_0(x) - (\omega_n - \omega_0)t + \phi_n)]. \tag{4}$$

Here $a_n(x)$, ω_n and ϕ_n represent the real amplitude, angular frequency, and initial phase for frequency component n of the primary wave motion, respectively. The L and U denote lower and upper frequency cut-off for the primary wave motion, which are assumed centered around, and in the vicinity of, some fixed frequency ω_0. The spatial derivative of the phase function defines a local wavenumber as in

$$\frac{\partial\psi_n(x)}{\partial x} = k_n(x) \approx k_0(x) + \left(\frac{\partial k}{\partial\omega}\right)_0(\omega_n - \omega_0) + O\Big((\omega_n - \omega_0)^2\Big). \tag{5}$$

The k_0 and ω_0 are related through the linear dispersion relation, ${\omega_0}^2 = gk_0 \tanh k_0 h$. In the following we will make use of

$$\begin{bmatrix}\Delta\omega_{n,m}\\ \Delta\phi_{n,m}\\ \Delta k_{n,m}\end{bmatrix} = \begin{bmatrix}\omega_n - \omega_m\\ \phi_n - \phi_m\\ k_n - k_m\end{bmatrix}, \quad C_{g0}(x) = \left(\frac{\partial\omega}{\partial k}\right)_0. \tag{6}$$

For sufficiently small $\Delta k_{n,m}h$, the subharmonic wave motion can be regarded as a slow modulation of depth and current. To describe this slow variation, we consider the depth-integrated and time-averaged (over the timescale of the short waves) equations of conservation of mass and momentum [e.g., *Phillips*, 1977, section 3.5; *Dingemans*, 1997, section 2.9]. If we limit ourselves to a 1DH situation, the linearized, combined set of equations for the lf surface elevation reads [e.g., *Mei and Benmoussa*, 1984; *Schäffer*, 1993]

$$\frac{\partial}{\partial x}\left(gh\frac{\partial}{\partial x}\eta^{(2)}(x,t)\right) - \frac{\partial^2}{\partial t^2}\eta^{(2)}(x,t) = -\frac{1}{\rho}\frac{\partial^2}{\partial x^2}S(x,t), \tag{7}$$

where h denotes water depth and $\eta^{(2)}(x, t)$ the subharmonic surface elevation response as a function of x and t. Gravitational acceleration is denoted by g. The S in the RHS of equation (7) denotes the radiation stress function which, from linear Stokes theory, may be expressed as

$$S(x,t) = \frac{1}{2}\rho g|A(x,t)|^2\left(\frac{2C_{g0}}{C_0} - \frac{1}{2}\right), \tag{8}$$

where C_{g0} and C_0 represent group and phase velocity, respectively, both in the linear approximation, corresponding to ω_0.

[43] In our evaluation of equation (7) we will consider a low-frequency response in the form of a summation of waves as in

$$\eta^{(2)}(x,t) = \sum_{m=1}^{U-L}\frac{1}{2}Z_m(x)\exp[-i\omega_m t] + *, \tag{9}$$

omitting the steady-state (zeroth harmonic) part of the response.

[44] Upon using equations (4), (8), and (9), we can express equation (7) for a frequency ω_m as

$$ghZ_{m,xx} + gh_x Z_{m,x} + \omega_m^2 Z_m = \left(F_m(x)\exp\left[i\int\kappa_m(x)\,dx\right]\right)_{xx}, \tag{10}$$

where x as a subscript denotes differentiation with respect to the spatial variable, $\kappa_m(x) \equiv \omega_m/C_{g0}(x)$, and $F_m(x)$ is a complex forcing amplitude:

$$F_m(x) = -g\left(\frac{2C_{g0}}{C_0} - \frac{1}{2}\right)\sum_{n=L}^{U-m}a_{m+n}a_n\exp\left[i\Delta\phi_{n,n-m}\right]. \tag{11}$$

We will omit frequency counters for convenience with the understanding that the following relations are considered for each frequency ω_m with $m \in \{1..(U-L)\}$.

[45] The spatial variability of the forcing wavenumber, $\kappa(x)$, and amplitude, $R(x)$, is governed by the variations in water depth. The latter is assumed small over a typical wavelength, and its order of magnitude is expressed by the ordering parameter

$$\beta = O\left(\frac{h_x}{\kappa h}\right) \ll 1. \tag{12}$$

The variations related to this slow variation of the medium can be made explicit by introduction of a slow space scale

$X = \beta x$. Furthermore, we expect both forcing and response to be functions with fast phase variations and slowly varying wavenumber and amplitude, suggesting a form of the solution as in

$$Z(X) = T(X)\exp\left[i\int \kappa(X)\beta^{-1}\,dX\right]. \tag{13}$$

Note that slow variations of amplitude and corrections to the phase function are incorporated in the complex amplitude T. The spatially varying phase shift between short-wave envelope and the low-frequency motion is recognized as

$$\psi_s = \arg\left(\frac{T}{F}\right). \tag{14}$$

Since the minus sign in the RHS of equation (7) is incorporated in the definition of F a non-zero ψ_s corresponds to a deviation from the π radians phase difference between short-wave envelope and low-frequency response as predicted by second-order Stokes theory. If, to a first approximation, we discard terms of $O(\beta^2)$, insertion of equation (13) into equation (10) yields

$$\mu T - i\beta\left(\frac{1}{h\kappa^2 T}\left(\kappa h T^2\right)_X - \frac{1}{gh\kappa^2 F}\left(\kappa F^2\right)_X\right) = \frac{F}{gh} + O\left(\beta^2\right), \tag{15}$$

where

$$\mu = \left(1 - \frac{C_{g0}^2}{gh}\right). \tag{16}$$

Physically, μ, represents a departure from resonance. The treatment of the problem greatly depends on the ratio $\beta\mu^{-1}$. The off-resonant case ($\beta\mu^{-1} = O(\beta)$) can be treated as a local response on a horizontal bottom with a small correction due to the inhomogeneity of the medium of order β. Clearly this approach breaks down for the near-resonant case for which $\beta\mu^{-1} \rightarrow O(1)$. In the latter case, equation (15) can be restated as an evolution equation for the forced wave. We will work out both approaches separately and compare results.

4.1. Local Response Corrections, $\beta\mu^{-1} = O(\beta)$

[46] To leading order, the response is given by

$$T^{(0)} = \frac{F}{gh\mu}, \tag{17}$$

which is the well-known solution for a forced subharmonic in shallow water propagating over a horizontal bottom as derived by *Longuet-Higgins and Stewart* [1962]. The bracketed superscript on T denotes the order (in terms of β) of the highest order terms included in the response. Including terms of $O(\beta)$ while substituting the leading order response in equation (15) yields

$$T^{(1)} = \frac{F}{gh\mu\left(1 - i\mu^{-1}Q\left(X, T^{(0)}, T_x^{(0)}\right)\right)}, \tag{18}$$

in which

$$Q = \frac{1}{\kappa}\left[\frac{2F_x}{F}(1-\mu) - \left(\frac{C_{g0,x}}{C_{g0}}(1-\mu) + \frac{h_x}{h} + \frac{2\mu_x}{\mu}\right)\right]. \tag{19}$$

In equation (19) the ordering parameter β is omitted and we returned to the single-scale (physical) spatial variable, x. From equations (14) and (18) we can write

$$T = \frac{F}{gh\mu}\exp[i\psi_s] + O\left(\beta^2\right), \tag{20}$$

where

$$\psi_s = \frac{Q}{\mu} + O\left(\beta^2\right). \tag{21}$$

Our expressions (19) and (21) can readily be evaluated, either by working out the terms containing the spatial derivatives or by numerically approximating them. The former approach is simplified considerably if we consider the case of a conservative bichromatic wave field with closely neighboring frequencies ω_1 and ω_2 as small perturbations around a mean frequency, ω_0. For this special case we can express the phase shift, ψ_s, analytically as

$$\psi_s = \frac{h_x}{\kappa h} f(k_0 h) + O\left(\beta^2\right), \tag{22}$$

with $f(k_0h)$ given in Appendix A. The expression (22) is a first-order approximation (in terms of depth variations) to the phase variation implied by equation (10) for the case $\beta\mu^{-1} = O(\beta)$.

4.2. Near-Resonance, $\beta\mu^{-1} = O(1)$

[47] In this case the perturbation approach breaks down and we restate equation (15) as

$$\beta T_X + i\frac{\kappa\mu}{2}T = -\beta\left(\frac{\kappa_X}{2\kappa} + \frac{h_X}{2h}\right)T + \frac{F}{2gh}\left[i\kappa + \frac{2\beta F_X}{F} + \frac{\beta\kappa_X}{\kappa}\right] + O\left(\beta^2\right), \tag{23}$$

which can be written as a coupled set of evolution equations for the lf-amplitude, $|Z| = |T|$, and phase shift, $\psi_s = \arg(TF^{-1})$, in the physical spatial variable x:

$$|Z|_x = \left(\frac{C_{g0,x}}{2C_{g0}} - \frac{h_x}{2h}\right)|Z| + \frac{|F|}{2gh} \cdot \left[\kappa\sin(\psi_s) + \left(\frac{2F_x}{F} - \frac{C_{g0,x}}{C_{g0}}\right)\cos(\psi_s)\right], \tag{24}$$

and

$$\psi_{s,x} = -\frac{\kappa\mu}{2} + \frac{|F|\kappa}{2gh|Z|}\left(\cos(\psi_s) - \frac{1}{\kappa}\left(\frac{2F_x}{F} - \frac{C_{g0,x}}{C_{g0}}\right)\sin(\psi_s)\right). \tag{25}$$

The latter equations represent a first-order approximation (in terms of β) both in the off-resonant region ($\beta\mu^{-1} = O(\beta)$) and in the region where the forcing problem is considered near-resonant ($\beta\mu^{-1} = O(1)$). For $h_x \rightarrow 0$ we have $\beta \rightarrow 0$ and in this limit, the set of equations (24)–(25) has steady solutions with $\psi_s = 0$ and $|Z| = |F|(gh\mu)^{-1}$.

[48] Validity demands the forced wave to remain of second order in magnitude as implicitly assumed by considering the evolution of the forced wave alone. The

effect of its evolution on the evolution of the primary waves is assumed small and is therefore neglected.

4.3. Model Intercomparison

[49] To verify our approximations we compare them to the exact solution to equation (10) for a plane slope, obtained through variation of parameters [e.g., *Van Leeuwen*, 1992; *Schäffer*, 1993], written as

$$Z = i\frac{\pi H_0^{(1)}(z)}{2gh_x}\left(C_1 - \int^x H_0^{(2)}(z')\frac{d^2}{dx^2}\widehat{S}(x')\,dx'\right) + i\frac{\pi H_0^{(2)}(z)}{2gh_x}\left(C_2 + \int^x H_0^{(1)}(z')\frac{d^2}{dx'^2}\widehat{S}(x')\,dx'\right), \qquad (26)$$

where $H_0^{(1)}$, $H_0^{(2)}$ are zeroth-order Hankel functions of the first and second kind, respectively, and $z = 2\omega x(gh)^{-1/2}$. The C_1 and C_2 are integration constants and $\hat{S}(x) = F\exp[i\int\kappa\,dx]$. The result of the numerical evaluation of equation (26) is referred to as exact linear response (ELR) and is taken as the reference solution to which the more approximate solutions are compared. The flat bottom response (equation (17)) as derived by *Longuet-Higgins and Stewart* [1962] will be referred to as local equilibrium response (LER). The local response correction and the coupled evolution equations are referred to as local equilibrium response correction (LERC) (equation (18)), and amplitude evolution response (AER) (equations (24)–(25)), respectively. The LERC model solution is taken as a boundary condition, at water sufficiently deep such that $\beta\mu^{-1} = O(\beta)$, for the numerical integration of the AER model. This integration is performed using a fourth-order, fixed step size, Runge-Kutta scheme.

[50] Figure 8 shows results for a bichromatic case with interacting frequencies $\{\omega_1, \omega_2\} = \{2.8, 3.6\}$ rad/s and bottom slope $h_x = 0.025$. A comparison between the ELR result and the approximate solutions for the phase shift, ψ_s/π, as a function of κh, is shown in Figure 8a. It can be seen that the LERC model is capable of correctly reproducing the small phase shifts occurring for larger κh; in shallower water ($O(\mu) \rightarrow O(\beta)$) the phase shift increases and clearly this perturbation approach can no longer be valid. From the same figure it can be seen that the AER model results are in very good agreement with the ELR solution for the range of κh shown.

[51] It is common practice to express spatial variations of the lf-amplitude in terms of the water depth as $|\eta_{lf}| \sim h^{-\alpha}$, where $\alpha = 1/4$ and $\alpha = 5/2$ correspond to Green's law and the shallow water limit of equation (17) (assuming conservative shoaling for the primary waves), respectively. In Figure 8b, α is shown as a function of $\kappa\ h$ for the LER, AER, and ELR models. It can be seen that the limit to which equation (17) tends is quite different from the one attained by the ELR model in shallow water. Spatial growth rates in shallow water for the latter are considerably smaller than suggested by the limit of equation (17). Growth rates produced by the approximating AER model are in excellent agreement with the ELR result.

[52] Note that we show a single case here and that, although we present the results in non-dimensional quantities, the results are not invariant to variations in h_x, $\Delta\omega$ and ω_0.

4.4. Comparison With Observations

[53] Comparisons between observed and computed (through evaluation of equations (24) and (25)) time lags for experiments 1A and 1C are shown in Figures 9a and 9b, respectively. For experiment 1C, the computed time lags are also shown in Figure 7a (line with circular markers). In Figures 9a and 9b the observed time lags (dotted line, square markers) correspond to the local minimum of the cross-correlation function nearest to $\tau = 0$ s for each position. The comparison is made for 0 m $\leq x \leq$ 20 m, since farther inshore the bar of negative correlation is no longer very distinct (for experiment 1A), and other physical processes than those accounted for in the linearized models are expected to become increasingly important.

[54] The numerical evaluations of equations (24)–(25) shown in Figures 9a and 9b are computed for the actual bottom profile with its boundary at the wave paddle ($x = -4.5$ m). The primary wave field is approximated as a bichromatic one, with its angular frequencies ω_0 and $\Delta\omega$ defined as 2π times the centroid frequency of the hf and lf

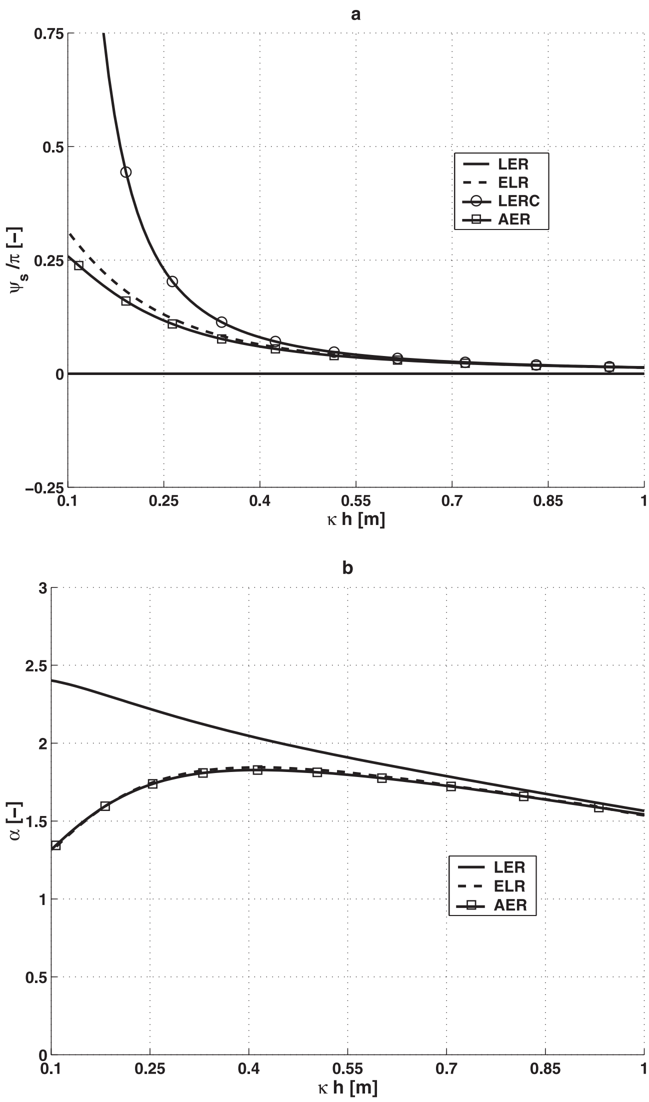

Figure 8. Comparison approximating models to ELR result. Bottom slope, $h_x = 0.025$ and interacting (angular) frequencies are $\{\omega_1, \omega_2\} = \{2.8, 3.6\}$ rad/s. (a) Phase shift, ψ_s/π, as a function of $\kappa h(\kappa = \Delta\omega/C_{g0})$. (b) Shoaling exponent α.

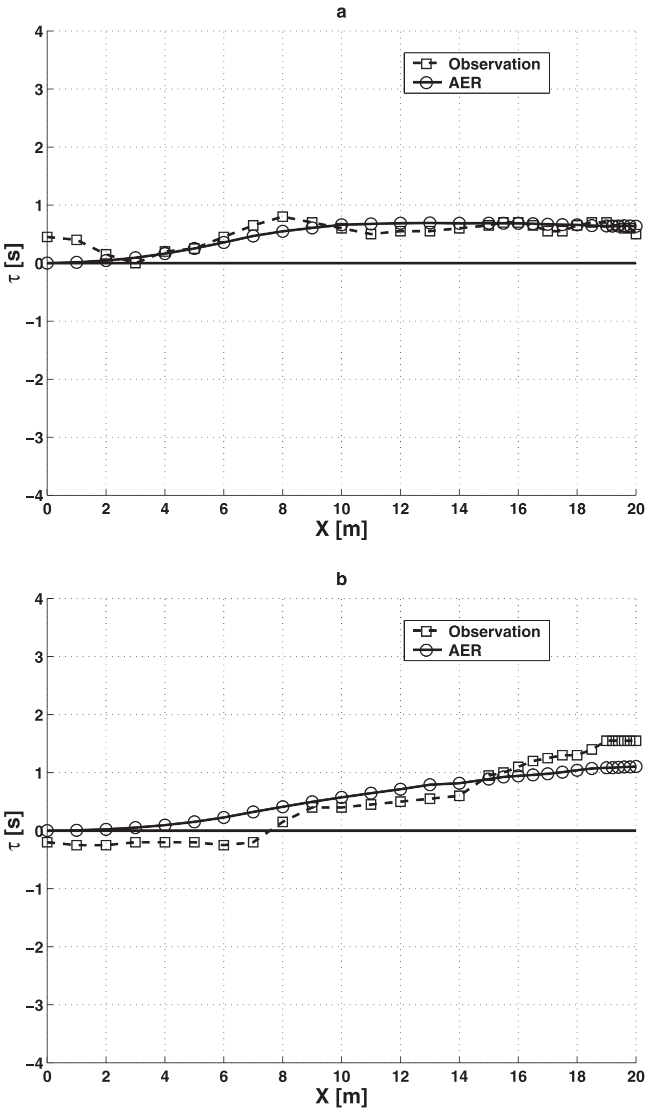

Figure 9. Comparison between observed time lag (corresponding to minimum of correlation function) and time lag computed with AER model. The primary wave field is approximated by a bichromatic one. (a) Experiment 1A, $\{\omega_1, \Delta\omega\} = \{3.0, 0.95\}$. (b) Experiment 1C, $\{\omega_1, \Delta\omega\} = \{2.4, 0.65\}$.

ranges of the spectrum (i.e., $\omega_0 = 2\pi(m_1/m_0)^{\mathrm{hf}}$ and $\Delta\omega = 2\pi(m_1/m_0)^{\mathrm{lf}}$, where m_i denotes the i^{th} moment of the frequency spectrum) resulting in $\{\omega_0, \Delta\omega\} = \{3.0, 0.95\}$ rad/s and $\{\omega_0, \Delta\omega\} = \{2.4, 0.65\}$ rad/s for experiments 1A and 1C, respectively. The observed spatial variation of the squared time-averaged hf-envelope was used as input for the spatial variation of the forcing amplitude. The computed phase shifts are related to time lag through $\tau = \psi_s/\Delta\omega$. It can be seen from Figures 9a and 9b that the computed time lags are in good qualitative agreement with the observed lags.

[55] In Figure 9a, for $x < 10$ m, we notice some wiggles in the observed time lag values, which are not reproduced. In Figure 9b the negative time lags for $x < 8$ m are not found in the numerical results. These mismatches may be caused by the presence of spurious free waves generated at the paddle, re-reflections or other differences in upwave boundaries that were not included in our present evaluation.

5. Discussion

[56] The bottom-slope induced phase lag of the forced lf-response with reference to the squared envelope, away from the equilibrium value of an exact opposite-phase relationship (π radians), has important dynamical consequences because it allows net work to be done on the lf-motion by the grouped short waves. Not only would this allow an increase of incident lf-energy flux while propagating in onshore direction, but would likewise result in a corresponding decrease of the incident primary wave energy flux.

[57] In the surf zone, only weak modulation (forcing) persists; combined with the increasing importance of dissipative processes, lf-energy fluxes decrease. Reflected lf-motion propagates in seaward direction, and in absence of forcing (and outside the dissipative region) its energy flux remains practically constant, which under the previously mentioned conditions yields Green's law for its amplitude decay. This variation in shoaling rates can result in a domination of the lf-wave field by incident waves in the nearshore region while farther offshore the relative magnitude of the reflected waves increases [e.g., *Sheremet et al.*, 2002] and eventually they become dominant [e.g., *Tucker*, 1950]. This inferred spatial variability of shoaling rates can explain the observed variability in intensity of the cross-correlation bars observed in Figure 5b.

[58] The occurrence of an energy transfer between short waves and forced lf-response has similar implications (but of opposite sign) for the energy balance for shoaling short waves, but this has not been taken into account so far. Nor has it ever been missed in comparison with observations. However, it should be noted that the lf-amplitudes in the shoaling zone are typically an order of magnitude smaller than those of the short waves, say 10%, so that an $O(1)$ change in the lf-energy then corresponds to only an imperceptible $O(10^{-2})$ sink in the short-wave energy balance. Needless to say, this approximation fails in very shallow water such as in the swash zone, where the lf-motion often is dominant.

6. Conclusions

[59] A detailed analysis has been made of a data set for one-dimensional shoaling and breaking random surface waves on a slope, and the attendant forced and free low-frequency motions. The high cross-shore resolution allowed a quasi-continuous space-time visualization of the propagation of the incident short-wave envelope as well as the incident (bound) and outgoing lf-waves, with a spatial detail that has not been available before. The results largely confirm and support existing notions concerning the propagation characteristics of the system of primary waves and forced subharmonics, as summarized below:

[60] 1. The cross-correlations of the hf-envelope signal observed at a fixed position with the hf-envelope signal at all other positions, confirm that the envelope propagates at a celerity close to C_{gp} (corresponding to f_p in the linear approximation); an inversion of groupiness of the hf-waves as they transit through the region of strong initial breaking is observed (i.e., on average the higher waves prior to break-

ing become the lower waves after breaking); no indication of reflection of hf-waves either on the slope (e.g., at the bar) or at the waterline is found.

[61] 2. The cross-correlations of the lf-wave signal observed at Station 1 ($x = 0$ m) with the lf-wave signal at all other positions show that incident lf-waves on average (over the length of the flume) propagate with celerity slightly smaller than C_{gp}; the lf-waves undergo significant and distinct reflection at the shoreline and after reflection propagate in offshore direction with celerity $\sqrt{gh}$. No indication of significant radiation of low-frequency waves from the region of initial breaking or the breaker bar was found; reflections of lf-motion at the breaker bar and the generation of lf-wave motion due to time variations of the initial breakpoint were apparently not effective.

[62] 3. The cross-correlations of lf-wave signal and squared short-wave envelope signal at the same positions show a shoreward increasing phase lag of the forced subharmonics behind the short-wave envelope while propagating over the sloping bottom. In the region of initial breaking the correlation at near-zero time lag is inverted from predominantly negative outside the surf zone to distinctly positive in the nearshore region; the inversion is mainly ascribed to depth modulation of the water depth through the presence of the low-frequency motion. Subharmonics that initially accompany the incident short-wave groups are released in the breaking process, reflected at the shoreline and subsequently propagate in offshore direction as free waves.

[63] A linear model is derived for the evolution of the forced subharmonics to first order in the relative bottom slope. The theoretically predicted phase lag is in fair agreement with the observed values. The corresponding theoretical amplitude evolution indicates that for the near-resonant lf-response over a sloping bottom, the local equilibrium response as derived by *Longuet-Higgins and Stewart* [1962] is not a proper approximation. It is generally not correct to interpret its asymptotic amplitude variation with depth, $h^{-5/2}$ (in the limit of small k_0h), as indicative of the shoaling amplification of bound lf-waves.

[64] The variability in shoaling rates for incident (forced) lf-wave motion, incident free and outgoing free waves with inclusion of an area of possible dissipation (surf zone), can result in a domination of incident wave motion in the nearshore region and an increasing relative importance of outgoing waves farther offshore.

Appendix A: Analytical Expression Phase Shift

[65] Consider the case $\beta\mu^{-1} = O(\beta)$, $\beta \ll 1$ and a primary wave field consisting of a bichromatic wave field with interacting frequencies ω_1 and ω_2 as small perturbations around a mean frequency, ω_0. The phase shift, ψ_s, can be expressed as

$$\psi_s = \frac{Q}{\mu} + O(\beta^2), \tag{A1}$$

where

$$Q = \frac{1}{\kappa}\left[\frac{2F_x}{F}(1-\mu) - \left(\frac{C_{g0,x}}{C_{g0}}(1-\mu) + \frac{h_x}{h} + \frac{2\mu_x}{\mu}\right)\right]. \tag{A2}$$

In the following, we will use $q \equiv k_0h$, $T \equiv \tanh(k_0h)$ for brevity and define

$$\begin{aligned}\gamma_1 &\equiv \frac{\left(T + q(1-T^2)\right)^2}{4qT},\\ \gamma_2 &\equiv (1-T^2)(1-qT),\\ \gamma_3 &\equiv T + 2q(1-T^2),\\ \gamma_4 &\equiv -\frac{q}{2T}(1-T^2)\left[T^3\right.\\ &\quad\left. + 2T(1-T^2) + q(1-T^2)^2\right].\end{aligned} \tag{A3}$$

We have the identities

$$\mu = 1-\gamma_1, \frac{\mu_x}{\mu} = \frac{h_x}{h}\frac{(\gamma_1-\gamma_2)}{(1-\gamma_1)}, \frac{C_{g0,x}}{C_{g0}} = \frac{h_x}{h}\frac{\gamma_2}{2\gamma_1}. \tag{A4}$$

If we take the primary wave field to be conservative we can further state

$$\frac{F_x}{F} = \frac{h_x}{h}\frac{\gamma_4}{\gamma_3\gamma_1}. \tag{A5}$$

Insertion of the latter expressions into equation (A1) yields, for the phase shift,

$$\psi_s = \frac{h_x}{\kappa h}f(k_0h) + O(\beta^2), \tag{A6}$$

where

$$\begin{aligned}f(k_0h) = &-\frac{1}{2(1-\gamma_1)}\\ &\cdot\left[2 + \gamma_2 + 4\left(\frac{(\gamma_1-\gamma_2)\gamma_3 - \gamma_4(1-\gamma_1)}{\gamma_3(1-\gamma_1)}\right)\right].\end{aligned} \tag{A7}$$

Notation

$A(x, t)$	short-wave envelope, (m);
$\eta(x, t)$	surface elevation, (m);
$\eta^{(1)}(x, t)$	primary wave surface elevation, (m);
$\eta^{(2)}(x, t)$	second-order surface elevation, (m);
$\eta^{\mathrm{lf}}(x, t)$	low-frequency surface elevation, (m);
$\eta^{\mathrm{hf}}(x, t)$	high-frequency surface elevation, (m);
$S(x, t)$	radiation stress function corresponding to primary wave field, (kg/s^2);
$\hat{S}_n(x)$	complex amplitude corresponding to nth frequency component of minus the radiation stress function per unit density, (m^3/s^2);
$F_n(x)$	slowly varying complex amplitude corresponding to nth frequency component of minus the radiation stress function per unit density, (m^3/s^2);
$a_n(x)$	real amplitude corresponding to nth frequency component of primary wave motion, (m);
$Z_n(x)$	complex amplitude corresponding to nth frequency component of second-order surface elevation, (m);
$T_n(x)$	slowly varying complex amplitude corresponding to nth frequency component of second-order surface elevation, (m);

ω_n angular frequency of nth frequency component, (1/s);
ω_0 center angular frequency defining bichromatic wave field description, (1/s);
f_p peak frequency, (1/s);
$\psi_n(x)$ space dependent part of phase function of nth frequency component of primary wave motion, (−);
$\psi_0(x)$ space dependent part of phase function of harmonic component corresponding to ω_0, (−);
$\psi_s(x)$ slowly varying phase shift between forced subharmonics and forcing envelope, (−);
$k_n(x)$ wavenumber of nth frequency component of primary wave motion, (1/m);
$k_0(x)$ wavenumber of harmonic component corresponding to ω_0, (1/m);
$k^{(1)}(x)$ characteristic wavenumber of primary wave motion, (1/m);
$\kappa(x)$ wavenumber of forced subharmonics, (1/m);
$C_{\mathrm{lf}}(x)$ actual velocity of observed low-frequency wave field, (m/s);
$C_A(x)$ actual velocity of observed short-wave envelope, (m/s);
$C_0(x)$ phase velocity corresponding to center angular frequency, ω_0, (m/s);
$C_{gp}(x)$ group velocity corresponding to peak frequency, (m/s);
$C_{g0}(x)$ group velocity corresponding to center angular frequency, ω_0, (m/s);
ϕ_n initial phase of nth frequency component of primary wave motion, (−);
$H_0^{(1)}$ zeroth-order Hankel function of first kind;
$H_0^{(2)}$ zeroth-order Hankel function of second kind;
g gravitational acceleration, (m/s^2);
μ resonant departure parameter, (−);
x cross-shore coordinate, positive onshore, (m);
X slowly scale cross-shore coordinate, positive onshore, (m);
β relative bottom slope, (−);
$\Delta\omega_{n,m}$ difference angular frequency, $\omega_n - \omega_m$, (1/s);
$\Delta\phi_{n,m}$ difference initial phase, $\phi_n - \phi_m$, (−);
$\Delta k_{n,m}$ difference wavenumber, $k_n - k_m$, (1/m);
t time, (s);
τ time lag, (s);
$R_{VY}(\tau)$ normalized cross-correlation function between signals V and Y, (−);
C_i ith integration constant, (m^2/s^2).

[66] **Acknowledgments.** The authors thank Marien Boers for putting his valuable data set at our disposal and for providing helpful support. Ap Van Dongeren' s time for this project was made available by WL/Delft Hydraulics within the framework of the Netherlands Centre for Coastal Research. We are indebted to A. J. Hermans for his useful comments and suggestions. Further, we wish to acknowledge Gert Klopman, Ad Reniers, Maarten Dingemans, and Tom Herbers for their many suggestions, corrections, and useful references related to the present work.

References

Baldock, T. E., and D. A. Huntley, Long wave forcing by the breaking of random gravity waves on a beach, *Proc. R. Soc. London, Ser. A*, *458*, 2177–2201, 2002.

Baldock, T. E., P. A. D. Huntley, T. Bird, and G. N. Bullock, Breakpoint generated surfbeat induced by bichromatic wave groups, *Coastal Eng.*, *39*, 213–242, 2000.

Bendat, J. S., and A. G. Piersol, *Random Data, Analysis and Measurement*, John Wiley, New York, 1986.

Biésel, F., Équations générales au second ordre de la houle irréguliér, *Houille Blanche*, *5*, 372–376, 1952.

Boers, M., Simulation of a surf zone with a barred beach: 1. Wave heights and wave breaking, *Commun. on Hydraulic and Geotech. Eng. Rep. 96-5*, 116 pp., Delft Univ. of Technol., Delft, Netherlands, 1996.

Bowen, A. J., and R. T. Guza, Edge waves and surf beat, *J. Geophys. Res.*, *83*, 1913–1920, 1978.

Bowers, E. C., Low frequency waves in intermediate water depths, paper presented at 23rd International Conference on Coastal Engineering, Am. Soc. of Civ. Eng., Venice, Italy, 1992.

Chu, V. H., and C. C. Mei, On slowly varying Stokes waves, *J. Fluid Mech.*, *41*, 873–887, 1970.

Dingemans, M. W., *Water Wave Propagation Over Uneven Bottoms: Nonlinear Wave Propagation*, World Sci., New York, 1997.

Dingemans, M. W., H. A. H. Petit, T. J. G. P. Meijer, and J. K. Kostense, Numerical evaluation of the third-order evolution equations for weakly nonlinear water waves propagating over uneven bottoms, in *Computer Modelling in Ocean Engineering*, pp. 361–370, A. A. Balkema, Brookfield, Vt., 1991.

Elgar, S., and R. T. Guza, Observations of bispectra of shoaling waves, *J. Fluid Mech.*, *161*, 425–448, 1985.

Elgar, S., T. H. C. Herbers, M. Okihiro, J. Oltman-Shay, and R. T. Guza, Observations of infragravity waves, *J. Geophys. Res.*, *97*, 15,573–15,577, 1992.

Gallagher, B., Generation of surf beat by non-linear wave interactions, *J. Fluid Mech.*, *49*, 1–20, 1971.

Hasselmann, K., On the non-linear energy transfer in a gravity-wave spectrum, *J. Fluid Mech.*, *12*, 481–500, 1962.

Herbers, T. H. C., and M. C. Burton, Nonlinear shoaling of directionally spread waves on a beach, *J. Geophys. Res.*, *102*, 21,101–21,114, 1997.

Herbers, T. H. C., S. Elgar, and R. T. Guza, Infragravity-frequency (0.005–0.05 Hz) motions on the shelf: I. Forced waves, *J. Phys. Oceanogr.*, *24*, 917–927, 1994.

Janssen, T. T., J. W. Kamphuis, A. R. Van Dongeren, and J. A. Battjes, Observations of long waves on a uniform slope, paper presented at 27th International Conference on Coastal Engineering, Am. Soc. of Civ. Eng., Sydney, 2000.

Klopman, G., and P. J. Van Leeuwen, An efficient method for the reproduction of non-linear waves, paper presented at 23rd International Conference on Coastal Engineering, Am. Soc. of Civ. Eng., Venice, 1992.

Kostense, J. K., Measurements of surf beat and setdown beneath wave groups, paper presented at 19th International Conference on Coastal Engineering, Am. Soc. of Civ. Eng., Houston, Tex., 1984.

Lancaster, P., and K. Šalkauskas, *Transform Methods in Applied Mathematics*, John Wiley, New York, 1996.

List, J. H., A model for the generation of 2-dimensional surfbeat, *J. Geophys. Res.*, *97*, 5623–5635, 1992.

Liu, P. L. F., A note on long waves induced by short wave groups over a shelf, *J. Fluid Mech.*, *205*, 163–170, 1989.

Longuet-Higgins, M., and R. W. Stewart, Radiation stress and mass transport in gravity waves, with application to "surf beats," *J. Fluid Mech.*, *13*, 481–504, 1962.

Mansard, E. P. D., and V. Barthel, Shoaling properties of bounded long waves, paper presented at 19th International Conference on Coastal Engineering, Am. Soc. of Civ. Eng., Houston, Tex., 1984.

Masselink, G., Group bound long waves as a source of infragravity energy in the surf zone, *Cont. Shelf Res.*, *15*, 1525–1547, 1995.

Mei, C. C., and C. Benmoussa, Long waves induced by short-wave groups over an uneven bottom, *J. Fluid Mech.*, *130*, 219–235, 1984.

Molin, B., On the generation of long period second order free waves due to changes in the bottom profile, *Rep. ifp:30167*, Inst. Francais du Petrol, Paris, 1982.

Munk, W. H., Surf beats, *Eos Trans. AGU*, *30*, 849–854, 1949.

Okihiro, M., R. T. Guza, and R. J. Seymour, Bound infragravity waves, *J. Geophys. Res.*, *97*, 11,453–11,469, 1992.

Oppenheim, A. V., and R. W. Schafer, *Discrete-Time Signal Processing*, Prentice-Hall, Old Tappan, N. J., 1989.

Phillips, O. M., *The Dynamics of the Upper Ocean*, 2nd ed., Cambridge Univ. Press, New York, 1977.

Reniers, A. J. H. M., A. R. van Dongeren, J. A. Battjes, and E. B. Thornton, Linear modeling of infragravity waves during Delilah, *J. Geophys. Res.*, *107*(C10), 3137, doi:10.1029/2001JC001083, 2002.

Roelvink, J. A., Surf beat and its effect on cross-shore profiles, Ph.D. dissertation, Delft Univ. of Technol., Delft, Netherlands, 1993.

Ruessink, B. G., The temporal and spatial variability of infragravity energy in a barred nearshore zone, *Cont. Shelf Res.*, *18*, 585–605, 1998.

Schäffer, H., Infragravity waves induced by short wave groups, *J. Fluid Mech.*, *247*, 551–588, 1993.

Sheremet, A., R. T. Guza, S. Elgar, and T. H. C. Herbers, Observations of nearshore infragravity waves: Seaward and shoreward propagating components, *J. Geophys. Res.*, *107*(C8), 3095, doi:10.1029/2001JC000970, 2002.

Symonds, G., and A. J. Bowen, Interactions of nearshore bars with incoming wave groups, *J. Geophys. Res.*, *89*, 1953–1959, 1984.

Symonds, G., D. A. Huntley, and A. J. Bowen, Two dimensional surfbeat: Long wave generation by a time-varying breakpoint, *J. Geophys. Res.*, *87*, 492–498, 1982.

Tucker, M. J., Surf beats: Sea waves of 1 to 5 min. period, *Proc. R. Soc. London, Ser. A*, *202*, 565–573, 1950.

Van Dongeren, A. R., Numerical modeling of quasi-3D nearshore hydrodynamics, Ph.D. dissertation, Univ. of Del., Newark, 1997.

Van Dongeren, A. R., and I. A. Svendsen, Nonlinear and 3D effects in leaky infragravity waves, *Coastal Eng.*, *41*, 467–496, 2000.

Van Dongeren, A. R., H. J. Bakkenes, and T. T. Janssen, Generation of long waves by short wave groups, paper presented at 28th International Conference on Coastal Engineering, Am. Soc. of Civ. Eng., Cardiff, Wales, 2002.

Van Leeuwen, P. J., Low frequency wave generation due to breaking waves, Ph.D. dissertation, Delft Univ. of Technol., Delft, Netherlands, 1992.

Van Leeuwen, P. J., and J. A. Battjes, A model for surfbeat, paper presented at 22nd International Conference on Coastal Engineering, Am. Soc. of Civ. Eng., Delft, Netherlands, 1990.

Veeramony, J., and I. A. Svendsen, Wave groups in the surf zone: Model and experiments, paper presented at 25th International Conference on Coastal Engineering, Am. Soc. of Civ. Eng., Orlando, Fla., 1996.

J. Battjes and T. T. Janssen, Section of Environmental Fluid Mechanics, Faculty of Civil Engineering and Geosciences, Delft University of Technology, P.O. Box 5048, 2600 GA Delft, Netherlands. (timtjanssen@yahoo.com)

A. R. van Dongeren, WL/Delft Hydraulics, P.O. Box 177, 2600 MH Delft, Netherlands. (ap.vandongeren@wldelft.nl)